International Symposium on Information Theory and its Applications, ISITA2004
Parma, Italy, October 10–13, 2004

EXIT Chart Analysis of Non-Regular Signal Constellation Sets for BICM-ID

Thorsten CLEVORN[1], Susanne GODTMANN[2], and Peter VARY[1]

[1]Institute of Communication Systems and Data Processing
RWTH Aachen University, Germany
{clevorn,vary}@ind.rwth-aachen.de

[2]Institute for Integrated Signal Processing Systems
RWTH Aachen University, Germany
godtmann@iss.rwth-aachen.de

Abstract

A key design element of bit-interleaved coded modulation with iterative decoding (BICM-ID) is the mapping of the bit patterns to the elements of the signal constellation set (SCS). Recently, we proposed mappings and new non-regular SCSs with superior asymptotic performance, i.e., lower error floors. These proposed mappings use signal constellation sets with less elements than the number of bit patterns to be transmitted and an appropriate assignment of the bit patterns to them. The puncturing introduced by the not one-to-one relation between assigned bit patterns and the elements of the SCS is compensated by the usage of extrinsic information obtained in the iterations. We further show the theoretical limits for the improvement of BICM-ID by this technique. Based on the mutual information concept of EXIT charts, a method is presented allowing easy determination of the achievable gains by different mappings for different kinds of channels. The results are confirmed by simulations.

1. INTRODUCTION

Bit-interleaved coded modulation (BICM) [1], [2] is a band-width efficient coded modulation scheme which increases the time-diversity and consequently is especially suited for Rayleigh fading channels. The key element of BICM is the serial concatenation of channel encoding, bit-interleaving, and multilevel modulations at the transmitter. In order to increase the performance of BICM in [3], [4] a feedback loop is added to the decoder, which results in a turbo-like decoding process. This new scheme is known as BICM with *iterative decoding* (BICM-ID). Another key element of BICM-ID is the usage of non-Gray mappings in the modulator. With these a significant improvement by the iterations can be achieved. By *mapping* we denote the whole design process of locating the possible positions of the channel symbols in the signal space, the *signal constellation set* (SCS), and assigning the possible bit patterns to these symbols.

In this paper we analyze the fundamentally new mappings with *non-regular* SCSs, which we proposed in [5]. These mappings owe their superior performance, i.e., their lower *error floor*, to a not one-to-one relation between channel symbols and assigned bit-patterns and, where appropriate, unequally distributed positions of the channel symbols in the signal space. The achievable performance gains are demonstrated by simulations and the convergence behavior is verified by EXIT charts [6], [7]. Additionally, a theoretical limit for the improvement of BICM-ID by the proposed technique is derived. Finally, the asymptotic performance, and consequently the achievable gains, of different mappings is analyzed using the concept of *mutual information* inherent in EXIT charts. In order to obtain these gains easily for different kinds of channels, a suitable method is presented.

2. THE BICM-ID SYSTEM

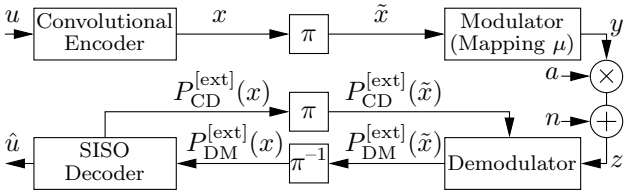

Figure 1: Baseband model of the BICM-ID system.

Fig. 1 depicts the baseband model of the BICM-ID system used in this paper. The data bits u are encoded by a convolutional encoder. The resulting encoded bits x are permuted by a pseudo-random bit-interleaver π to $\tilde{x}$. The modulator maps an interleaved bit pattern $\underline{\tilde{x}}_t = [\tilde{x}_t^{(1)}, \ldots \tilde{x}_t^{(I)}]$ of I bits, e.g., $I=3$ in case of 8PSK, according to a mapping rule μ to a complex channel symbol $y_t \in \mathbb{C}$ out of the SCS $\mathcal{Y}$

$$y_t = \mu(\underline{\tilde{x}}_t) \quad . \tag{1}$$

The respective inverse relation is denoted by μ^{-1}, with

$$\underline{\tilde{x}}_t = \mu^{-1}(y_t) = [\mu^{-1}(y_t)^{(1)}, \ldots \mu^{-1}(y_t)^{(I)}] \quad . \tag{2}$$

The channel symbols are normalized to an average energy of $E_s = E\{\|y_t\|^2\} = 1$. The transmitted symbols y_t are faded by the Rayleigh distributed coefficients a_t with $E\{\|a_t\|^2\} = 1$. In this paper we assume that these coefficients are known at the receiver, i.e., perfect knowledge of the channel state information (CSI). Next, complex white Gaussian noise $n_t = n_t' + jn_t''$ with a known power spectral density of $\sigma_n^2 = N_0$ ($\sigma_{n'}^2 = \sigma_{n''}^2 = N_0/2$) is added. Thus, the received channel symbols z_t can be written as

$$z_t = a_t y_t + n_t \quad . \tag{3}$$

At the receiver the demodulator (DM) computes *extrinsic* probabilities $P_{\mathrm{DM}}^{[\mathrm{ext}]}(\tilde{x})$ for each bit $\tilde{x}_t^{(i)}$ being $b \in \{0,1\}$ according to [4]

$$P_{\mathrm{DM}}^{[\mathrm{ext}]}(\tilde{x}_t^{(i)} = b) \sim \sum_{\hat{y} \in \mathcal{Y}_b^i} P(z_t|\hat{y}) P_{\mathrm{CD}}^{[\mathrm{ext,i}]}(\hat{y}) \quad , \tag{4}$$

$$\text{with} \quad P_{\mathrm{CD}}^{[\mathrm{ext,i}]}(\hat{y}) \triangleq \prod_{j=1, j\neq i}^{I} P_{\mathrm{CD}}^{[\mathrm{ext}]}\left(\tilde{x}_t^{(j)} = \bar{\mu^{-1}}(\hat{y})^{(j)}\right) \quad . \tag{5}$$

Each $P_{\mathrm{DM}}^{[\mathrm{ext}]}(\tilde{x})$ consists of the sum over all channel symbols $\hat{y}$ for which the i^{th} bit of the corresponding bit pattern $\underline{\tilde{x}} = \bar{\mu^{-1}}(\hat{y})$ is b. These symbols form the subset $\mathcal{Y}_b^i$ with $\mathcal{Y}_b^i = \{\mu([\tilde{x}^{(1)}, \ldots \tilde{x}^{(I)}]) | \tilde{x}^{(i)} = b\}$. In the first iteration the feedback probabilities $P_{\mathrm{CD}}^{[\mathrm{ext}]}(\tilde{x})$ are initialized as equiprobable. With the channel used in (3), $P(z_t|\hat{y})$ is given by

$$P(z_t|\hat{y}) = \frac{1}{\pi\sigma_n^2} \exp\left(-\frac{\|z_t - a_t\hat{y}\|^2}{\sigma_n^2}\right) \quad . \tag{6}$$

After appropriately deinterleaving the $P_{\mathrm{DM}}^{[\mathrm{ext}]}(\tilde{x})$ to $P_{\mathrm{DM}}^{[\mathrm{ext}]}(x)$, the $P_{\mathrm{DM}}^{[\mathrm{ext}]}(x)$ are fed into a Soft-Input Soft-Output (SISO) channel decoder (CD), which computes both *extrinsic* probabilities $P_{\mathrm{CD}}^{[\mathrm{ext}]}(x_t^{(i)})$ of the encoded bits $x_t^{(i)} = \{0,1\}$ in addition to the preliminary estimated decoded data bits $\hat{u}$. For the next iteration the $P_{\mathrm{CD}}^{[\mathrm{ext}]}(x)$ are interleaved again to $P_{\mathrm{CD}}^{[\mathrm{ext}]}(\tilde{x})$.

3. PERFORMANCE ANALYSIS

Since for non-iterative BICM Gray mappings are optimal [2], we concentrate on the analysis of the performance in the iterative case with BICM-ID. If the channel is sufficiently good and enough iterations are carried out we can assume *error-free feedback* (EFF) [4], i.e., we assume that the feedback $P_{\mathrm{CD}}^{[\mathrm{ext}]}(\hat{x})$ for all bits except the one currently considered is correct with perfect reliability (best case). Using the perfectly reliable *extrinsic* information in the EFF results in a BPSK decision between the two channel symbols y and $\check{y}$, which posses identical bit patterns except for the position i of the currently considered bit. On the right side of Fig. 2 the resulting BPSK decisions are depicted for the 8PSK-SSP (Semi-Set-Partitioning) mapping [4].

For a Rayleigh fading channel the performance bound for the bit-error rate (BER) P_b of BICM-ID is derived in [4]. The asymptotic behavior, i.e., the *error floor*, of the BER can be described by

$$\log_{10} P_b \approx \frac{-d_{\mathrm{Ham}}(\mathcal{C})}{10} \left[\left(R \cdot \check{d}_h^2(\mu)\right)_{\mathrm{dB}} + \left(\frac{E_b}{N_0}\right)_{\mathrm{dB}}\right] + const. \tag{7}$$

The minimum Hamming distance $d_{\mathrm{Ham}}(\mathcal{C})$ of the channel code $\mathcal{C}$ with rate r defines the slope of the bound. Whereas $\check{d}_h^2(\mu)$ is the *harmonic mean* of the *squared Euclidean distances* of the BPSK decisions with EFF. The product of the information rate $R = rI$ and the *harmonic mean* $\check{d}_h^2(\mu)$ determines an E_b/N_0 offset of the bound, i.e., a horizontal offset in a BER vs. E_b/N_0 plot. $E_b = E_s/R$ is the energy per information bit. For a mapping with I bits the *harmonic mean* $\check{d}_h^2(\mu)$ is given by

$$\check{d}_h^2(\mu) = \left(\frac{1}{I2^I} \sum_{i=1}^{I} \sum_{b=0}^{1} \sum_{y \in \mathcal{Y}_b^i} \frac{1}{\|y - \check{y}\|^2}\right)^{-1} . \tag{8}$$

In case of non-iterative BICM, i.e., no feedback, $\check{d}_h^2(\mu)$ has to be replaced by the harmonic mean $\bar{d}_h^2(\mu)$. $\bar{d}_h^2(\mu)$ is computed similar to $\check{d}_h^2(\mu)$, except that $\check{y}$ is replaced by $\bar{y}$, where $\bar{y}$ denotes the nearest neighbor y with an inverted bit at position i, whatever the rest of the bit pattern contains.

The ratio $\mathcal{G}(\mu) = (\check{d}_h^2(\mu)/\bar{d}_h^2(\mu)^{[\max]})_{\mathrm{dB}}$ is called *offset gain* [4] and describes the possible gain of BICM-ID with a certain mapping with respect to the optimum mapped non-iterative BICM. The optimum mapping for the BICM is usually a Gray mapping, i.e., for $I = 3$ the 8PSK-Gray mapping with $\bar{d}_h^2(\mu)^{[\max]} = \bar{d}_h^2(\text{8PSK-Gray}) = 0.766$. The *offset gain* $\mathcal{G}(\mu)$ and the corresponding $\check{d}_h^2(\mu)$ serve as key indicators for the evaluation of the theoretically achievable performance of mappings in the *error floor* region with BICM-ID [4], [5]. Note, the *offset gain* $\mathcal{G}(\mu)$ is independent of the channel code and can consequently be achieved by any code. Mappings with *regular* 8PSK SCS were investigated in [4]. Semi-Set-Partitioning (SSP) mapping depicted in Fig. 2 has the largest $\check{d}_h^2(\text{8PSK-SSP}) = 2.877$, which yields an *offset gain* of $\mathcal{G}(\text{8PSK-SSP}) = 5.74$ dB.

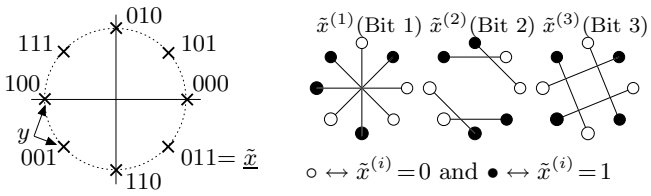

Figure 2: 8PSK-SSP with signal-pair distances $\|y-\check{y}\|$.

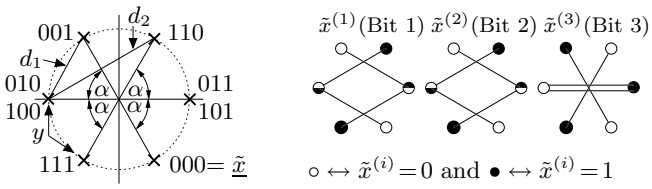

Figure 3: α-6PSK$_{I=3}$ with signal-pair distances $\|y-\check{y}\|$.

4. NON-REGULAR SIGNAL CONSTELLATION SETS

In order to increase the *offset gain*, i.e., lower the *error floor*, we proposed in [5] the usage of new mappings μ with SCSs with less than the usual 2^I different channel symbols y for bit patterns $\underline{\tilde{x}}$ with I bits and, where appropriate, an unequal distribution of the channel symbols in the signal space.

4.1. α-6PSK mapping for $I = 3$

As example in this paper we consider the α-6PSK$_{I=3}$ mapping depicted in Fig. 3, which maps $2^{I=3} = 8$ different bit patterns $\underline{\tilde{x}}$ to 6 channel symbols y. The angle α defines the angle between certain channel symbols on the unit circle with respect to the origin. Thus, by changing α different mappings can be obtained. With this α-6PSK$_{I=3}$ mapping twice two bit patterns $\underline{\tilde{x}}$ are mapped to the same channel symbol y, i.e., $\underline{\tilde{x}}_{1,2} = [010], [100] \Rightarrow y = -1$ and $\underline{\tilde{x}}_{1,2} = [011], [101] \Rightarrow y = +1$. In the first iteration this results in an automatic partial puncturing of these addends in (4). At the bit positions i where the bit patterns differ, $\tilde{x}_1^{(i)} \neq \tilde{x}_2^{(i)}$, the addends with $\hat{y}_{1,2} = \mu(\underline{\tilde{x}}_{1,2})$ are distributed equally weighted to $P_{\mathrm{DM}}^{[\mathrm{ext}]}(\tilde{x}^{(i)} = 0)$ and $P_{\mathrm{DM}}^{[\mathrm{ext}]}(\tilde{x}^{(i)} = 1)$, since $P_{\mathrm{CD}}^{[\mathrm{ext,i}]}(\hat{y}_1) = P_{\mathrm{CD}}^{[\mathrm{ext,i}]}(\hat{y}_2)$. This partial puncturing of the addends implies a severe degradation of the performance in the initial iteration. We still have $R = rI$, but without the feedback loop the demodulator cannot obtain all the transmitted information of the 3 encoded bits per channel symbol y, even for $E_b/N_0 \to \infty$.

However, if the E_b/N_0 is sufficiently high the decoder can cope the introduced puncturing and generates improving feedback $P_{\mathrm{CD}}^{[\mathrm{ext,i}]}(\hat{y})$. This feedback will be different for $\underline{\tilde{x}}_1$ and $\underline{\tilde{x}}_2$, i.e., $P_{\mathrm{CD}}^{[\mathrm{ext,i}]}(\mu(\underline{\tilde{x}}_1)) \neq P_{\mathrm{CD}}^{[\mathrm{ext,i}]}(\mu(\underline{\tilde{x}}_2))$, and thus it improves the computation of $P_{\mathrm{DM}}^{[\mathrm{ext}]}(\tilde{x})$ by compensating (or reducing) the partial puncturing. With EFF the demodulator for the α-6PSK$_{I=3}$ mapping is able to extract the complete information of the 3 encoded bits per channel symbol y, similar to any 8PSK mapping. Note, all $\underline{\tilde{x}}$ mapped to one y must differ in at least two bits, because otherwise for a single different bit i, we would have $\check{y} = y$ at this bit, resulting in $\check{d}_h^2(\mu) = 0$. The *extrinsic* feedback information for the single different bit being 0 or 1 would be always identical.

At high E_b/N_0 and a sufficient number of iterations the feedback may finally converge to EFF, the necessary assumption for the computation of $\check{d}_h^2(\mu)$ in (8). For the angles $\alpha = 60°$ and $\alpha = 45°$ we can obtain *offset gains* of $\mathcal{G}(60°\text{-6PSK}_{I=3}) = 6.30$ dB and $\mathcal{G}(45°\text{-6PSK}_{I=3}) = 6.71$ dB, which are higher than the one of 8PSK-SSP mapping. Thus, the two α-6PSK$_{I=3}$ mappings will outperform 8PSK-SSP mapping by 0.56 dB resp. 0.97 dB when the E_b/N_0 is such high that in both cases the bound is reached. Note, in case of a relatively high target BER, the mapping with the largest *offset gain* may not be the best choice, since it might only be superior at a BER below the target BER. However, the goal of *non-regular* SCSs is to lower the *error floor*, which corresponds to higher *offset gains*. More *non-regular* SCSs are presented in [5].

4.2. BPSK mapping for $I \geq 2$

Reducing the number of possible channel symbols y to 2, i.e., using a *regular* BPSK SCS, is not feasible since no bit pattern assignment for $I \geq 2$ exists which does not violate one of the two necessary conditions for the bit patterns $\underline{\tilde{x}}$ of the channel symbols y. On the one hand the bit patterns assigned to one channel symbols must differ in at least 2 positions. On the other hand the assigned bit patterns must have common bits for at least for some channel symbols. Otherwise all bits are automatically punctured in the first iteration and no usable feedback can be generated. Note that these conditions are contrary for all *non-regular* SCSs. With a better fulfillment of the first one, i.e., more than 2 different bits in the bit patterns assigned to one channel symbol, the asymptotic performance can often be improved. But consequently these bit patterns have less common bits, resulting in a worse performance in the first iteration.

4.3. Theoretical Limit

In this section we derive the theoretical maximum *offset gain*. First a system with $I = 3$ bits per channel symbol is considered. The extreme case of $\alpha \to 0$

in Fig. 3 results on the one hand in the *Euclidean* distance $d_1 \to 0$, meaning that $E_b/N_0 \to \infty$ is required to have improving feedback. On the other hand, looking at the asymptotic performance with EFF, we have $d_2 \to 2$ which yields in $\check{d}_h^2(\mu) \to 4$. The corresponding OG is $\mathcal{G}_{I=3}^{[\max]} = 7.18$ dB. With EFF all signal-pairs resemble now a BPSK SCS with $y = \pm 1$. This is obviously the best possible case for a symbol energy of $E_s = 1$ and therefore a bound for the obtainable OG with BICM-ID and $I = 3$. Due to the similarity of the SCSs we will denote this bound in the following as BPSK bound [5]. Obviously, the value $\check{d}_h^2(\mu) = 4$ marks also an upper limit for systems with $I \neq 3$. The corresponding maximum achievable *offset gain* $\mathcal{G}_I^{[\max]}$, however, additionally depends on $\bar{d}_h^2(\mu)^{[\max]}$, which differs depending on I and is usually achieved with Gray or near-Gray mappings.

5. BER SIMULATION RESULTS

Table 1 lists $\check{d}_h^2(\mu)$ and the respective *offset gains* $\mathcal{G}(\mu)$ for the considered mappings with $I = 3$. Fig. 4 depicts the results of bit-error rate (BER) simulations comparing the different mappings for a block size of 12000 information bits per frame and 30 iterations. An 8-state, rate-1/2, feed-forward convolutional code with generator polynomials $\{15, 17\}_8$ and $d_{\text{Ham}}(\mathcal{C}) = 6$ serves as channel code. As expected, the *waterfall* region of the α-6PSK$_{I=3}$ mappings occurs at higher E_b/N_0 due to the automatic puncturing in the first iteration. However, the *error floors* of the α-6PSK$_{I=3}$ mappings show the superior performance predicted by their larger *offset gains*. Below a BER of $\sim 10^{-5}$ the 60°-6PSK$_{I=3}$ mapping outperforms 8PSK-SSP by approximately the difference between their *offset gains*.

Table 1: $\check{d}_h^2$ and $\mathcal{G}$ for mappings with $I = 3$ bits.

mapping μ	$\check{d}_h^2(\mu)$	offset gain $\mathcal{G}(\mu)$
8PSK-SSP [4] (Fig. 2)	2.877	5.74 dB
60°-6PSK$_{I=3}$ (Fig. 3, $\alpha = 60°$)	3.273	6.30 dB
45°-6PSK$_{I=3}$ (Fig. 3, $\alpha = 45°$)	3.589	6.71 dB
BPSK bound (Fig. 3, $\alpha \to 0°$)	4	7.18 dB

6. EXIT CHART ANALYSIS

EXIT (*extrinsic* information transfer) charts [6], [7] are a powerful tool to analyze the convergence behavior of iterative systems utilizing the Turbo principle, i.e., systems exchanging and refining *extrinsic* information. The capabilities of the components, in our case the demodulator (DM) and the SISO channel decoder (CD), are analyzed separately. The *extrinsic mutual information* $\mathcal{I}^{[\text{ext}]}$ obtained by each component for a certain *a priori mutual information* $\mathcal{I}^{[\text{apri}]}$ is determined. Both, $\mathcal{I}^{[\text{ext}]}$ and $\mathcal{I}^{[\text{apri}]}$, are calculated on the basis of the actual data and the available information, *extrinsic* or *a priori*, for the data. Since the *extrinsic* information of one component serves as input *a priori* information for the other component, the two resulting EXIT characteristics are plotted in a single graph with swapped axes. The EXIT characteristic of the demodulator, i.e., of the considered mapping, depends on the E_b/N_0 of the channel. Contrariwise, the EXIT characteristic of the channel decoder is independent of the E_b/N_0 since it has no access to the received channel symbols z.

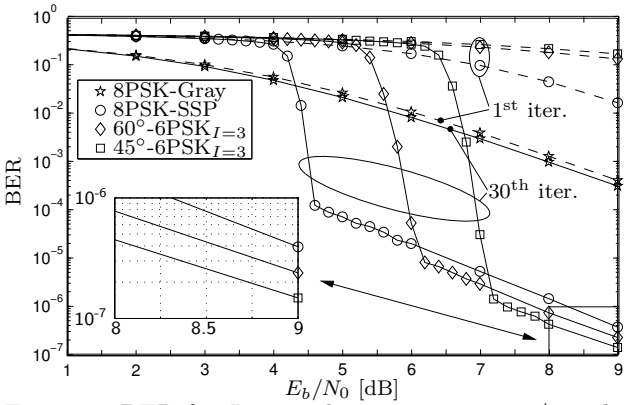

Figure 4: BER for $I = 3$ with a 8-state, rate-1/2 code.

6.1. Analysis of the Convergence Behavior

The EXIT chart in Fig. 5 depicts the EXIT characteristics for the mappings and the channel decoder used in Fig. 4 for $E_b/N_0 = 6$ dB. As visible the EXIT characteristic of 8PSK-Gray mapping is almost horizontal, which prohibits any significant gain by iterations. The EXIT characteristics of the other mappings exhibit noticeable slopes, allowing improvement by numerous iterations. The depicted EXIT trajectory for the 60°-6PSK$_{I=3}$ mapping proves that despite the introduced *non-regular* SCS the proposed mappings feature the usual iterative convergence behavior.

6.2. Analysis of the Asymptotic Behavior

The performance analysis in Section 3 and the development of the *non-regular* SCSs in Section 4 are not based on the convergence behavior but on the asymptotic behavior. To compute the achievable *offset gains* the assumption of *error-free feedback* (EFF) is made. In the EXIT charts this EFF corresponds to $\mathcal{I}_{\text{DM}}^{[\text{apri}]} = 1$. Accordingly, information on the asymptotic behavior, i.e., the *error floor*, is available on the right vertical axis $\mathcal{I}_{\text{DM}}^{[\text{apri}]} = 1$. The area under the EXIT character-

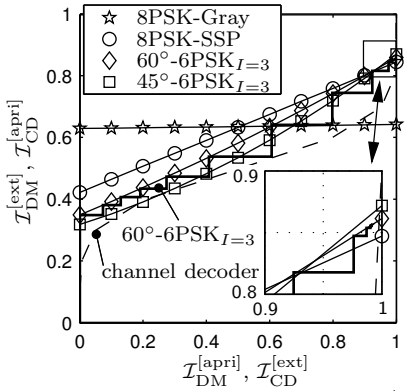

Figure 5: EXIT charts for Fig. 4 at $E_b/N_0 = 6$ dB.

istics of the mappings with *non-regular* SCSs is obviously smaller than the one of the mappings with regular SCSs, indicating a loss of information during the convergence process when using *non-regular* SCSs [8]. However, as visible in the enlargement in Fig. 5 the order of $\mathcal{I}_{\mathrm{DM}}^{[\mathrm{ext}]}$ of the mappings reverses for $\mathcal{I}_{\mathrm{DM}}^{[\mathrm{apri}]} \approx 1$. Thus, with EFF, i.e., when the *error floor* is reached, the presented *non-regular* SCSs provide more *extrinsic mutual information* than the regular SCSs.

With the used demodulator the values of $\mathcal{I}_{\mathrm{DM}}^{[\mathrm{ext}]}$ for $\mathcal{I}_{\mathrm{DM}}^{[\mathrm{apri}]} = 1$ can be calculated numerically. The EFF at $\mathcal{I}_{\mathrm{DM}}^{[\mathrm{apri}]} = 1$ consists of $P_{\mathrm{CD}}^{[\mathrm{ext,i}]}(y) \in \{0.0, 1.0\}$ and taking the Rayleigh fading into account the *mutual information* $\mathcal{I}_{\mathrm{DM}}^{[\mathrm{ext}]}(\mathcal{I}_{\mathrm{DM}}^{[\mathrm{apri}]} = 1)$ can be determined by [7]

$$\mathcal{I}_{\mathrm{DM}}^{[\mathrm{ext}]}(\mathcal{I}_{\mathrm{DM}}^{[\mathrm{apri}]} = 1) = \frac{1}{I 2^I} \sum_{i=1}^{I} \sum_{y \in \mathcal{Y}} \int_{0}^{\infty} P(a) \iint_{-\infty}^{\infty} P(z|y,a) \cdot \mathrm{ld}\, \frac{P(z|y,a)}{P(z)} \mathrm{d}z' \mathrm{d}z'' \mathrm{d}a \quad , \tag{9}$$

with $z = z' + jz''$, the Rayleigh distribution $P(a) = 2a \exp(-a^2)$, the two-dimensional conditional probability density function

$$P(z|y,a) = \frac{1}{\pi \sigma_n^2} \exp\left(-\frac{\|z - ay\|^2}{\sigma_n^2} \right) \tag{10}$$

and $P(z) = \frac{1}{2}(P(z|y,a) + P(z|\check{y},a))$. As introduced in Section 3 the channel symbol $\check{y}$ posses the same bit pattern as y except for an inverted bit at position i. Since with EFF the signal space degenerates to one-dimensional BPSK modulations, the double integral on z in the computation of $\mathcal{I}_{\mathrm{DM}}^{[\mathrm{ext}]}(\mathcal{I}_{\mathrm{DM}}^{[\mathrm{apri}]} = 1)$ can be simplified to a single integral on z' by modifying (10) with $\check{d} = \|y - \check{y}\|$ to

$$P(z'|\check{d},a) = \frac{1}{\sqrt{2\pi}\sigma_{n'}} \exp\left(-\frac{|z' - a\check{d}/2|^2}{2\sigma_{n'}^2} \right) \quad . \tag{11}$$

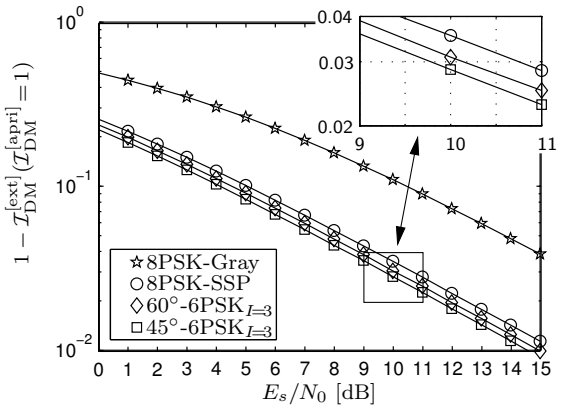

Figure 6: $\mathcal{I}_{\mathrm{DM}}^{[\mathrm{ext}]}$ for mappings with EFF, i.e., $\mathcal{I}_{\mathrm{DM}}^{[\mathrm{apri}]} = 1$; Rayleigh channel.

For an increasing E_s/N_0 the value of $\mathcal{I}_{\mathrm{DM}}^{[\mathrm{ext}]}(\mathcal{I}_{\mathrm{DM}}^{[\mathrm{apri}]} = 1)$ converges towards 1. For better visualization we plotted $1 - \mathcal{I}_{\mathrm{DM}}^{[\mathrm{ext}]}(\mathcal{I}_{\mathrm{DM}}^{[\mathrm{apri}]} = 1)$ versus E_s/N_0 in Fig. 6. As visible at high E_s/N_0 the almost constant horizontal offsets between the different mappings match the differences between the *offset gains* $\mathcal{G}$ listed in Table 1. The numerically obtained curves coincide with the curves obtained when evaluating the simulated EXIT characteristics at $\mathcal{I}_{\mathrm{DM}}^{[\mathrm{apri}]} = 1$.

Since the presented procedure described above to obtain $\mathcal{I}_{\mathrm{DM}}^{[\mathrm{ext}]}(\mathcal{I}_{\mathrm{DM}}^{[\mathrm{apri}]} = 1)$ either by numerical calculation or Monte-Carlo simulation is independent of the channel features this technique to acquire the achievable performance gains of BICM-ID is also applicable for other channels than the considered Rayleigh channel. For a numerical calculation the conditional probability density function of the channel has to be known. Fig. 7 depicts the results of Monte-Carlo simulations for a non-fading AWGN channel.

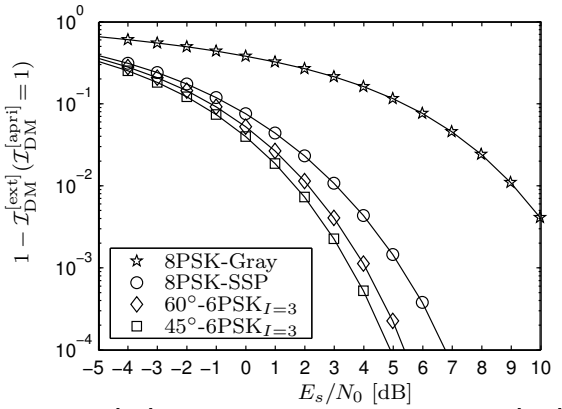

Figure 7: $\mathcal{I}_{\mathrm{DM}}^{[\mathrm{ext}]}$ for mappings with EFF, i.e., $\mathcal{I}_{\mathrm{DM}}^{[\mathrm{apri}]} = 1$; AWGN channel.

6.3. Analysis of the Non-Iterative Behavior

Furthermore, not only at $\mathcal{I}_{\mathrm{DM}}^{[\mathrm{apri}]}=1$ the feedback is predetermined, also at $\mathcal{I}_{\mathrm{DM}}^{[\mathrm{apri}]}=0$ the feedback values $P_{\mathrm{CD}}^{[\mathrm{ext}]}(\tilde{x})$ are perfectly known, i.e., $P_{\mathrm{CD}}^{[\mathrm{ext}]}(\tilde{x})=0.5$ for equiprobable bits and consequently $P_{\mathrm{CD}}^{[\mathrm{ext,i}]}(y)=1/2^{I-1}$.

Modifying (9) appropriately $\mathcal{I}_{\mathrm{DM}}^{[\mathrm{ext}]}(\mathcal{I}_{\mathrm{DM}}^{[\mathrm{apri}]}=0)$ can be determined by

$$\mathcal{I}_{\mathrm{DM}}^{[\mathrm{ext}]}(\mathcal{I}_{\mathrm{DM}}^{[\mathrm{apri}]}=0) = \frac{1}{2I}\sum_{i=1}^{I}\sum_{b=0}^{1}\int_{0}^{\infty}P(a)\iint_{-\infty}^{\infty}P_{\Sigma}(z|y,a) \cdot \mathrm{ld}\,\frac{P_{\Sigma}(z|y,a)}{P_{\Sigma}(z)}\mathrm{d}z'\mathrm{d}z''\mathrm{d}a \quad , \tag{12}$$

with

$$P_{\Sigma}(z|y,a)=\sum_{y\in\mathcal{Y}_b^i}P(z|y,a)P_{\mathrm{CD}}^{[\mathrm{ext,i}]}(y)=\frac{1}{2^{I-1}}\sum_{y\in\mathcal{Y}_b^i}P(z|y,a) \tag{13}$$

and

$$P_{\Sigma}(z)=\frac{1}{2^I}\sum_{y\in\mathcal{Y}}P(z|y,a) \quad . \tag{14}$$

In Fig. 8 the values for $\mathcal{I}_{\mathrm{DM}}^{[\mathrm{ext}]}(\mathcal{I}_{\mathrm{DM}}^{[\mathrm{apri}]}=0)$ are depicted for the different mappings and a Rayleigh channel. Again the curves coincide with the ones obtained by Monte-Carlo simulations. As expected the curves for the α-6PSK$_{I=3}$ mappings converge towards 2/3 due to in average 1/3 of the bits being automatically punctured without feedback as explained in Section 4. Moreover, 8PSK-Gray mapping always exhibits the highest values $\mathcal{I}_{\mathrm{DM}}^{[\mathrm{ext}]}(\mathcal{I}_{\mathrm{DM}}^{[\mathrm{apri}]}=0)$ identifying it as the optimum mapping for the non-iterative case. For low E_s/N_0 the curves of the α-6PSK$_{I=3}$ mappings and the 8PSK-SSP mapping approach each other. This behavior can also be found in Fig. 4, in which these three mappings exhibit an alike performance in the first iteration at low E_s/N_0 while 8PSK-Gray mapping is significantly superior.

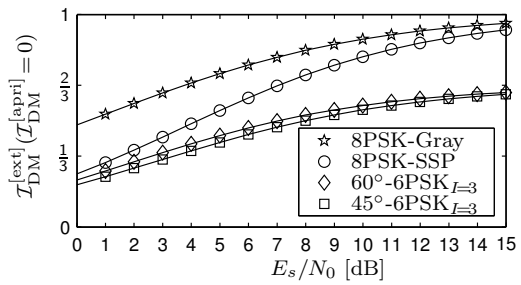

Figure 8: $\mathcal{I}_{\mathrm{DM}}^{[\mathrm{ext}]}$ for mappings without feedback, i.e., $\mathcal{I}_{\mathrm{DM}}^{[\mathrm{apri}]}=0$, and a Rayleigh channel.

7. CONCLUSION

In this paper the improved capabilities of BICM-ID when using fundamentally new mappings with *non-regular signal constellation sets* are analyzed. These mappings have less channel symbols than possible bit patterns. Thus, more than one bit pattern may be assigned to one channel symbol. Also the position of the channel symbols are not necessarily equally distributed anymore. By this technique larger *offset gains* for ideal feedback are achievable in comparison to previously known mappings. Simulations demonstrate that the theoretically predicted performance of the novel mappings can be achieved. Furthermore a bound for the achievable improvement by this technique is derived. Based on the concept of *mutual information* in EXIT charts a method is presented to easily obtain the possible *offset gains* with BICM-ID by either numerical calculation or simulation. This proposed method is not restricted to Rayleigh channels, but it is applicable to other kinds of channels.

References

[1] E. Zehavi, "8-PSK Trellis Codes for a Rayleigh Channel," *IEEE Trans. Comm.*, pp. 873–884, May 1992.

[2] G. Caire, G. Taricco, and E. Biglieri, "Bit-Interleaved Coded Modulation," *IEEE Trans. Inform. Theory*, pp. 927–946, May 1998.

[3] X. Li and J. A. Ritcey, "Bit-Interleaved Coded Modulation with Iterative Decoding," *IEEE Comm. Lett.*, pp. 169–171, Nov. 1997.

[4] X. Li, A. Chindapol, and J. A. Ritcey, "Bit-Interleaved Coded Modulation With Iterative Decoding and 8PSK Signaling," *IEEE Trans. Comm.*, pp. 1250–1257, Aug. 2002.

[5] T. Clevorn and P. Vary, "Iterative Decoding of BICM with Non-Regular Signal Constellation Sets," in *5th Internat. ITG Conf. on Source and Channel Coding (SCC)*, Erlangen, Germany, Jan. 2004.

[6] S. ten Brink, "Designing Iterative Decoding Schemes with the Extrinsic Information Transfer Chart," *International Journal of Electronics and Communications (AEÜ)*, pp. 389–398, Dec. 2000.

[7] S. ten Brink, "Convergence Behavior of Iteratively Decoded Parallel Concatenated Codes," *IEEE Trans. Comm.*, pp. 1727–1737, Oct. 2001.

[8] A. Ashikhmin, G. Kramer, and S. ten Brink, "Extrinsic information transfer functions: model and erasure channel properties," *IEEE Trans. Inform. Theory, to appear 2004.*